Spatial Statistics 34 (2019) 100268

Contents lists available at ScienceDirect

Spatial Statistics

journal homepage: www.elsevier.com/locate/spasta

Statistical characterization of flow field structure in evolving braided gravel beds

Domenica Mirauda, Annamaria De Vincenzo, Marilena Pannone *

School of Engineering, University of Basilicata, 10 Ateneo Lucano Avenue, 85100 Potenza, Italy

ARTICLE INFO

Article history:
Received 28 February 2017
Accepted 13 October 2017
Available online 25 October 2017

Keywords:
River velocity statistics
Bed elevation statistics
Evolving braided configuration
Equilibrium and pre-equilibrium conditions
Laboratory experiments

ABSTRACT

Braided rivers quickly vary their geometry, modifying their boundaries and floodplains. Therefore, flooding of a braided stream is typically associated with high hydrologic risk in the surrounding areas or alluvial valleys. A forecast of these morpho-hydrodynamic processes is therefore essential when managing the environmental and economic impact of flood events. A few studies in the past demonstrated that open channels spontaneously tend to establish and maintain an equilibrium state that corresponds to a specific level of cross-sectional velocity entropy. The present study analyses for the first time the relationship between bank-full flow (described by measures of velocity entropy and second-order spatial statistics) and bed topography (described in terms of bed elevation second-order spatial statistics) in gravel-bed braided rivers at cross-sectional scale, in both equilibrium and pre-equilibrium conditions. Based on the outcome of suitable laboratory experiments, we found that, in gravel bed braided rivers, longitudinal equilibrium during floods is associated with a periodic-like spatial minimization of normalized cross-sectional velocity entropy. This periodic-like minimization of cross-sectional velocity entropy (and statistical variance) corresponds to a periodic-like maximization of normalized bed elevation variance, according to general theories on longitudinal river profile evolution. Additionally, bed evolution occurs by both entropy minima/maxima appearance and growth and entropy minima/maxima longitudinal migration.

* Corresponding author.
E-mail address: marilena.pannone@unibas.it (M. Pannone).

https://doi.org/10.1016/j.spasta.2017.10.004
2211-6753/

Notation

A	Flow area
B	Flume width
ξ	Monotonic velocity variation coordinate
D	Representative sediment diameter
δ	Wetted bed elevation function
Δ	Mean cross-sectional bed profile
E	Relative energy
ε_δ	Bed elevation semi-variogram
f	State variable probability density function
g	Acceleration due to gravity
h	Flow depth
H_u	Velocity distribution entropy
k	Boltzmann constant
κ	von-Kàrmàn constant
M	Entropic parameter
ν	Water kinematic viscosity
q	Unit-width flow rate
Q	Flow rate
Re_0^*	Grain Reynolds number
ρ	Water density
ρ_s	Sediment density
σ_δ^2	Bed elevation variance
σ_u^2	Velocity variance
S	Gibbs' (thermodynamic) entropy
τ^*	Dimensionless shear stress
u	Flow longitudinal velocity
$\overline{u}$	Depth-averaged velocity
u^*	Shear velocity
$u_{\max}$	Maximum velocity
U	Mean cross-sectional velocity
x	Longitudinal coordinate
y	Transverse coordinate
z	Vertical coordinate

1. Introduction

Braided rivers rapidly change their geometry, modifying their boundaries and floodplains and carrying out large amounts of solutes, floating logs and sediments. Consequently, flooding of a braided stream considerably increases the hydrologic risk in the surrounding areas or alluvial valleys, where anthropic infrastructures like roads, viaducts, bridges, aqueducts and gas pipelines are often located. Gravel bed changes occur almost exclusively in response to bank-full flow. An evaluation of the evolving river morpho-hydrodynamic conditions that is as fast and reliable as possible is therefore of paramount importance when managing structural damage and human safety risk associated with a flood event (e.g. Kreibich et al., 2009). Unfortunately, uncertainty is inherent in hydraulic studies (such as in the investigation of river flow and morphology or sediment/solute concentration and shear stress dynamics), due to both intrinsic process randomness and operators' ignorance or inability to understand and deal with it. The traditional approach to hydraulic studies using the conservation laws of Fluid Mechanics (equation of continuity, momentum and energy) is deterministic. Despite advances made with the deterministic approach, it still presents serious problems and limitations

that may perhaps be addressed probabilistically. In the field of fine suspended load and solute concentration dynamics, several recent analytical/numerical studies dealt with the problem in terms of spatial moments based on Eulerian or Lagrangian stochastic approaches (Pannone, 2010a, b, 2012a, b, 2014; Pannone and De Vincenzo, 2015). A different way to address uncertainty issues in Environmental Hydraulics by resorting to statistical tools may be represented by the use of an originally thermodynamic variable, i.e. the information entropy (e.g. Shannon, 1948).

A few studies in the past demonstrated that, under a wide range of flow conditions, open channels tend to establish and maintain an equilibrium state that corresponds to a single specific level of cross-sectional velocity entropy. Chiu (1991) found that erodible channels tend to stabilize and to achieve the maximum possible velocity entropy for given hydrological constraints by enhancing erosion and suspended load, and that larger values of maximum entropy are associated with streams characterized by more uniform flow conditions.

Chiu and Said (1995) showed for a variety of flow rates and depths that, in order to achieve this maximum-entropy equilibrium state, an erodible channel typically evolves modulating several hydraulic and geometric characteristics (cross-sectional shape, slope, roughness, local axis curvature and, hence, velocity distribution and sediment transport). On the other hand, non-erodible channels can respond to variations in the general hydrological conditions by adjusting only water depth and, hence, velocity distribution. Therefore, due to the reduced number of freedom degrees, non-erodible channels are characterized by a wider range of possible equilibrium-velocity entropy values (e.g. Luo and Singh, 2011).

Although typically evaluated at cross-sectional scale, entropy may vary along the channel due to the locality of the morpho-hydrodynamic characteristics, which were showed to strongly affect entropy level (Moramarco et al., 2008).

Laboratory tests in a flume, carried out by Greco et al. (2014) and by Greco and Mirauda (2015a, b) under steady flow conditions, homogeneous bed roughness and, hence, homogeneous distribution of near-bed irregularities, showed that the level of velocity entropy is dominated by local near-bed conditions. Specifically, it emerged that, in the regime of large to intermediate roughness, the ratio of average to maximum velocity (or, in statistical terms, the ratio of the ensemble mean to one of the extremes of the cross-sectional statistical distribution, which is straightforwardly related to entropy) is a logarithmic function of the ratio of depth to roughness. Conversely, in the regime of small roughness that relationship exhibits a more marked uncertainty.

Overall, the above-cited works show that cross-sectional velocity entropy is a suitable global indicator of local flow conditions and may therefore be used to classify the different types of channel and the corresponding typical equilibrium states.

The present study analyses for the first time the relationship between bank-full flow field (described by measures of velocity entropy and second-order spatial statistics) and bed topography (described in terms of bed elevation second-order spatial statistics) in gravel-bed braided rivers at cross-sectional scale, both in equilibrium and in pre-equilibrium conditions. Note that, in this case, "equilibrium conditions" means reach-scale bed trend coinciding with reach-scale free surface trend, as well as sediment discharge and bar geometric dimensions characterized by nearly constant values (Parker, 2003).

The aim of the analysis was to investigate braided bed pre-asymptotic temporal evolution, verifying the possibility to map the emergence of gravel bars by the detection of peculiar longitudinal variations exhibited by velocity entropy and local bed elevation variance. Indeed, in situations where direct measurements are expensive and potentially dangerous (e.g. Mirauda et al., 2011), as well as affected by uncertainty due to the high level of turbulence and to critical-state oscillations, such an estimate would rely on easier geometric surveys only. For that purpose, the data collected during high grain Reynolds number experiments conducted at University of Basilicata (De Vincenzo et al., 2016) were processed. Additionally, the entropic approach by Chiu (1991) and Chiu and Said (1995) was extended to unsteady non-uniform flows like those taking place in evolving braided beds in bank-full conditions. This modified entropic approach allowed defining space/time dependent cross-sectional velocity moments that can be evaluated based on a single, easily estimated parameter. Space/time dependent moments of random functions (such as the normalized variances/coefficients of variation squared of velocity and bed elevation) are representative of non-stationary inhomogeneous stochastic

processes. Thus, in a very complex scenario such as the evolution of gravel bed toward braided equilibrium, we suggest to forecast and monitor bed evolution in terms of space–time variations of bed elevation and velocity variance (or entropy).

2. Theoretical background

The term entropy was introduced by Clasius and first applied to the statistical interpretation of physical phenomena by Boltzmann in 1871. Entropy is widely used in chemical thermodynamics, which analyses the variations of energy that are involved in chemical reactions. A basic thermodynamic assumption is that any physical system, if undisturbed, tends to spontaneously evolve toward a stable condition, known as equilibrium. At equilibrium the entropy, which is a measure of the disorder of the system, is the maximum possible for given constraints. Entropy is also a central concept in thermal and quantum physics, where it is representative of the ensemble of quantum states (Jaynes, 1957; Kittel and Kroemer, 1980). The development of the idea of entropy of random variables and processes is due to Shannon (1948) and laid the foundation for the information theory and the modern age of ergodic theory. Indeed, entropy and related information measures provide suitable descriptions of the long-term behaviour of random processes (Gray, 2013). Despite the formal equivalence of the corresponding mathematical definitions (except for the presence of Boltzmann's constant k in the thermodynamic case), there is an important difference between thermodynamic and information entropy. The information entropy:

$$H = -\sum_i p_i \ln p_i \tag{1}$$

where the probability p_i concerns a discrete statistical distribution of events, can in principle be calculated whatever this distribution is referred to. Conversely, the thermodynamic entropy:

$$S = -k\sum_i p_i \ln p_i \tag{2}$$

specifically refers to thermodynamic probabilities (i.e. to the probability of different possible thermodynamic states) and is proportional to the number of dynamic states of the system that are possible on a molecular scale for the given macroscopic thermodynamic properties. Nevertheless, if the probabilities in question are thermodynamic probabilities, a connection can be made between the two: the (reduced) Gibbs entropy $\sigma = S/k$ can simply be seen as the amount of Shannon's information needed to define the detailed microscopic state of the system given its macroscopic description. As a consequence, searching for the equilibrium distributions of statistical mechanics (i.e. the Boltzmann distribution) by maximizing Gibbs' entropy subject to appropriate constraints can be seen as something not unique to thermodynamics, but rather as a general principle for all types of statistical inference where one is looking for the most uninformative probability distribution subject to certain constraints on the behaviour of its average descriptors. In other words, information entropy should be viewed as an evolution of the idea of thermal entropy.

An important application of the concept of information entropy is found in the field of Bayesian inference and disambiguation of inverse problems (e.g. Jaynes, 1983, 1984; Woodbury and Ulrich, 1993). An emblematic example of specific application in the field of environmental Fluid Mechanics is represented by the introduction of a dilution index expressed in terms of concentration distribution entropy, for the investigation of groundwater pollutant dynamics (Kitanidis, 1994; Pannone and Kitanidis, 1999). One of the first, landmark applications to river morphology is due to Leopold and Langbein (1962). Based on their theoretical results, the most probable (and therefore expected) sequence of energy losses in successive units of river length corresponds to a uniform increase of bed morphology entropy in each of these units.

This apparently broad range of possible definitions for the term entropy has a key unifying factor. Indeed, in all of its uses entropy measures a "number of possibilities".

In the case of continuous statistical distributions (which are of interest in the present study), entropy is mathematically defined as follows:

$$H(X) = -\int f(X)\ln[f(X)]\,dX \tag{3}$$

where $f(X)$ indicates the probability density function of the state variable, so that $f(X)dX$ is the probability of the variable itself being between X and $X + dX$. According to Shannon's theory, maximum entropy means maximum information inferred from the data (messages) about the state variable X. Based on Eq. (3), this translates into maximum uncertainty in X before measurements. To determine $f(X)$ (i.e., the *a priori* probability density function of variable X) that maximizes $H(X)$, one may resort to the method of the calculus of variations (e.g. Gelfand and Fomin, 2000). For a state variable ranging between two known generic limits X_1 and X_2, one has to search for the maximum of

$$H(X) = -\int_{X_1}^{X_2} f(X) \ln[f(X)]\, dX \tag{4}$$

subject to a set of m constraints:

$$\int_{X_1}^{X_2} \Theta_j(X, f)\, dX = K_j \quad j = 1, \ldots, m \tag{5}$$

where Θ_j indicates a generic function of the random variable X and its probability density f. The shape of function f is determined as the zero of the following linear combination of derivatives:

$$\frac{\partial I(X, f)}{\partial f} + \sum_{j=1}^{m} \lambda_j \frac{\partial \Theta_j(X, f)}{\partial f} \tag{6}$$

where λ_j indicate Lagrangian multipliers and $I(X, f) = -f(X) \ln[f(X)]$.

In the present open-channel flow application, the maximization of the velocity entropy evaluated along the flow depth h:

$$H(u) = -\int_0^{u_{\max}} f(u) \ln[f(u)]\, du \tag{7}$$

subject to the following constraints:

$$\int_0^{u_{\max}} f(u)\, du = 1 \tag{8}$$

and

$$\int_0^{u_{\max}} uf(u)\, du = \overline{u} \tag{9}$$

yields

$$f(u) = \exp(\lambda_1 - 1) \exp(\lambda_2 u) = \left(h \frac{du}{dz}\right)^{-1} \tag{10}$$

and

$$H(u) = -\lambda_1 + 2 - u_{\max} \exp(\lambda_1 - 1 + \lambda_2 u_{\max}) \tag{11}$$

where

$$\exp(\lambda_1 - 1) = \frac{\lambda_2}{\exp(\lambda_2 u_{\max}) - 1} \tag{12}$$

and

$$\overline{u} = \frac{u_{\max} \exp(\lambda_2 u_{\max})}{\exp(\lambda_2 u_{\max}) - 1} - \frac{1}{\lambda_2}. \tag{13}$$

In the above equations, $u = u(z)$ is the depth-variable velocity, u_{max} is the maximum of the distribution, $\overline{u}$ indicates local depth-average and z is the vertical Cartesian coordinate. Note that Eq. (10) implies the cumulative distribution function $F(u) = \int_0^u f(u)\, du = z/h$ and, therefore, $u_{max} = u(h)$.

Based on these results, and after suitable algebraic manipulations and generalizations, Chiu (1991) derived the following cross-sectional velocity distribution:

$$u(y,z) = \frac{u_{\max}}{M} \ln\left\{1 + [\exp(M) - 1]\frac{\xi - \xi_0}{\xi_{\max} - \xi_0}\right\} \tag{14}$$

where y indicates channel transverse coordinate and $\xi = \xi(y,z)$ is a special function defined so that u increases monotonically with it and ξ_0 and ξ_{max} indicate the values of ξ where $u = 0$ and $u = u_{max}$, respectively. The contour map of function ξ represents the family of cross-sectional isovels (Chiu and Chiou, 1986). Eq. (14) applies also in the more general case of maximum located somewhere in the cross-section at $z < h(y)$, due to intense cross-sectional secondary currents (e.g. Nezu et al., 1993) and free surface-induced turbulence anisotropy. Additionally, the "entropic" parameter M is related to the Lagrangian multipliers by the following expressions:

$$\lambda_1 = 1 + \ln\left\{\frac{[M\exp(M) - \exp(M) + 1]}{U[\exp(M) - 1]^2}\right\} \tag{15}$$

and

$$\lambda_2 = \frac{M}{u_{\max}} \tag{16}$$

where U (mean cross-sectional velocity) replaces $\overline{u}$.

Despite the introduction of a generalized cross-sectional coordinate, velocity distribution (14) cannot apply to channel sections that are not simply connected domains or in case of non-uniform flow conditions. In braided beds, cross-sections are highly irregular and often partialized due to the presence of large bars. Additionally, longitudinally uniform flow can only occur in an average sense. The outlined approach can still be valid (Eqs. (7)–(13) and (15)–(16)) with $u = u(x,y,z)$ (where x indicates channel longitudinal coordinate) and $U(x) = Q/A(x) = Q/\left[B\overline{h}(x)\right]$ (where Q is the total flow rate, A the longitudinally varying flow area, B the flume width and $\overline{h}$ the mean cross-sectional flow depth). Note that, in this case, Eq. (7) should be rewritten as follows:

$$H_u(x) = -\int_0^{u_{\max}(x)} f(u|x)\ln[f(u|x)]\,du \tag{17}$$

and the (cross-sectional) maximization should be carried out based on the conditional probability density function $f(u \mid x)$.

3. Methodology

In the present study, which focuses on braided bed temporal evolution toward equilibrium, we started from estimating the ratio $U(x,t)/u_{\max}(x,t)$, where $u_{\max}(x,t) = \max_y u_{\max}(x,y,t)$, by means of the continuity equation for incompressible fluids in steady flow conditions $Q = UB\overline{h} = \text{const}$ and the local application of Prandtl–von Kàrmàn's logarithmic law for rough turbulent flows (Yalin, 1992):

$$\frac{u(x,y,z,t)}{u_*(x,t)} = \frac{1}{\kappa}\ln\left[\frac{(z|x,y,t)}{2D_{50}}\right] + 8.5. \tag{18}$$

In Eq. (18) and in what follows, $\kappa = 0.41$ indicates von-Kàrmàn constant, u_* shear velocity and D_{50} the average sediment diameter. From (18) one obtains

$$\frac{u_{\max}(x,y,t)}{u_*(x,t)} = \frac{u(x,y,h,t)}{u_*(x,t)} = \frac{1}{\kappa}\ln\left[\frac{h(x,y,t)}{2D_{50}}\right] + 8.5. \tag{19}$$

Indeed, although the position of the local velocity peak does not necessarily coincide with the free surface, its value is well approximated by classical wall-turbulence laws like (18), which invariably predict the maximum at $z = h$. The efficacy of Eq. (18) was independently validated by verifying that it suitably reconstructed the longitudinal profile of the mean cross-sectional velocity:

$$U(x,t) = \frac{Q}{A(x,t)} = \frac{1}{B}\int_0^B \overline{u}(x,y,t)\,dy \tag{20}$$

where

$$\begin{aligned}\overline{u}(x,y,t) &= \frac{u_*(x,t)}{h(x,y,t)-2D_{50}}\int_{2D_{50}}^{h(x,y,t)}\left\{\frac{1}{k}\ln\left[\frac{(z|x,y,t)}{2D_{50}}\right]+8.5\right\}dz \\ &\cong u_*(x,t)\left\{\frac{1}{k}\ln\left[\frac{0.368h(x,y,t)}{2D_{50}}\right]+8.5\right\}.\end{aligned} \tag{21}$$

Then, the non-uniform, unsteady flow generalization of Eqs. (13), (15) and (16):

$$\frac{U(x,t)}{u_{\max}(x,t)} = \frac{\exp[M(x,t)]}{\{\exp[M(x,t)]-1\}} - \frac{1}{M(x,t)} \tag{22}$$

$$\lambda_1(x,t) = 1+\ln\left\{\frac{[M(x,t)\exp(M(x,t))-\exp(M(x,t))+1]}{U(x,t)[\exp(M(x,t))-1]^2}\right\} \tag{23}$$

$$\lambda_2(x,t) = \frac{M(x,t)}{u_{\max}(x,t)} \tag{24}$$

along with Eq. (11), allowed us to evaluate the entropic parameter M along the flume axis for five experimental runs at three different running times, and to assess the time-dependent longitudinal variation of the normalized cross-sectional velocity entropy:

$$\begin{aligned}H_u(x,t) &= H\left[\frac{u(x,y,z,t)}{u_{\max}(x,t)}\right] = H[u(x,y,z,t)]-\ln[u_{\max}(x,t)] \\ &= 1+\ln\left\{\frac{\exp[M(x,t)]-1}{M(x,t)}\right\}-\frac{M(x,t)\exp[M(x,t)]}{\exp[M(x,t)]-1}\end{aligned} \tag{25}$$

as well as the time-dependent longitudinal variation of the normalized variance of velocity:

$$\begin{aligned}\frac{\sigma_u^2(x,t)}{U^2(x,t)} &= \frac{1}{U^2(x,t)}\int_0^{u_{\max}(x,t)}[u(x,y,z,t)-U(x,t)]^2 f(u|x,t)\,du \\ &= \frac{\{\exp[M(x,t)]-1\}\left\{\exp[M(x,t)]\left[M^2(x,t)-2M(x,t)+2\right]-2\right\}}{\{\exp[M(x,t)][M(x,t)-1]+1\}^2}-1\end{aligned} \tag{26}$$

where

$$f(u|x,t) = \frac{M(x,t)}{u_{\max}(x,t)\{\exp[M(x,t)]-1\}}\exp\left[\frac{M(x,t)\,u}{u_{\max}(x,t)}\right]. \tag{27}$$

Finally, to investigate the relationship between flow field and bed topography heterogeneity, we evaluated the normalized variance of wetted-bed elevation function δ based on the experimental measurements:

$$\frac{\sigma_\delta^2(x,t)}{\Delta^2(x,t)} = \frac{1}{\Delta^2(x,t)\,B}\int_0^B[\delta(x,y,t)-\Delta(x,t)]^2 dy \tag{28}$$

where Δ indicates mean cross-sectional bed profile. The assumption underlying Eq. (28) is that the flume represented one of the statistically similar stream-tubes characterized by zero side shear stress in which a wide river can be subdivided. In this case, the spatial average performed over width B is equivalent to the ensemble mean performed over all the possible statistical realizations of function $\delta(x,t)$ at any given time. The soundness of such assumption was experimentally verified by evaluating the ratio of active to total width, which was always smaller than one (0.5 on average). Active width is the portion of bed width that is effectively involved in transport and morphological changes; therefore, it can be considered as a sort of instantaneous transverse correlation scale (l_δ) characterizing $\delta(x,y,t)$ (De Vincenzo et al., 2016). In these conditions, with $l_\delta < B$, laboratory flume width could be assumed as statistically representative of bed elevation transverse distribution.

The aim of such investigation was the attempt to establish and discuss the qualitative relationship between the two statistical moments ((26) and (28)), thus verifying the possibility to capture the essential elements of flow field structure by a simple bed map.

Table 1
Summary of the experimental conditions.

Run	Q (m^3/s)	S_0	S_{0SB}	S_{eq}	t_{eq} (h)
R1	0.0444	0.014	0.084	0.007	46
R2	0.031	0.013	0.067	0.012	167
R3	0.036	0.0135	0.067	0.011	168
R4	0.0254	0.027	0.0566	0.015	261
R9	0.053	0.0104	0.032	0.01	261

4. Laboratory survey procedure

The characteristics of the experimental device employed in the present study (Fig. 1) were chosen to simulate the typical morpho-dynamic processes taking place in a gravel-bed braided stream, with the corresponding geometric and hydraulic parameters selected according to Froude similitude (Peakall et al., 1996; Young and Warburton, 1996). The laboratory flume (16.7 m long and 1 m wide) consisted of a metal structure confined by Plexiglas sidewalls. It was inserted into a re-circulating system made of (1) an upstream rectangular tank, connected to a 2.3 m long sediment supplying basin by a curved Creager weir; (2) an overhead travelling crane; (3) two pumps; (4) two downstream collecting tanks connected to each other by a v-shaped weir. The sediment supplying basin was fed with water by the upstream tank and with gravel by a sediment feeder mounted on the travelling crane. The mixture of sediment and water coming from the supplying basin gradually saturated the flume bottom until the achievement of the design initial slope under the given flow rate. The downstream collecting tanks separated the exceeding sediment from the water, which was then re-circulated by the two pumps.

Each run was designed requiring that the dimensionless shear stress $\tau^* = \gamma R_H j/(\gamma - \gamma_s)\, D_{50}$ (where R_H is the hydraulic radius, j the unit energy loss and γ and γ_s water and sediment specific weight, respectively) over the initially flat bottom would be larger than the value corresponding to incipient transport (0.047). Additionally, it was required that the initial grain Reynolds number $\mathrm{Re}_0^* = u_* D_{50}/\nu$ (with ν indicating water kinematic viscosity) would be much larger than 70 ($632 \leq \mathrm{Re}_0^* \leq 711$) according to Yalin's criterion for rough-turbulent flow (Yalin, 1971). Fluvial gravel utilized to fill flume bottom was characterized by $D_{50} = 9$ mm, $D_{10} = 5$ mm, $D_{90} = 13$ mm and different grain shapes. The runs differed from each other in terms of flow rate and initial slope of flume bottom and sediment-supplying basin. See Table 1 for a summary of the experimental conditions, where S_0 indicates initial flume slope, S_{eq} equilibrium bed slope, S_{0SB} initial supplying basin slope and t_{eq} the running time needed to achieve equilibrium.

The equilibrium grain Reynolds number ranged from 601 to 710. Therefore, it was always much larger than the grain Reynolds numbers reported by most of previous laboratory experiments performed with sand (Viparelli and Pica, 1967; Young and Davies, 1991; Zarn, 1997; Bertoldi et al., 2009) and consistent with the condition of fully turbulent flow. The relative mean cross-sectional depth $\overline{h}/D_{50}$, which is one of the controlling factors in braiding and bar development, ranged from 7 to 8.8 at equilibrium. The ratio of active width to average depth $B_{act}/\overline{h}$ varied between 20 and 23.8 and was comparable with that reported in previous large-scale laboratory experiments (Ashmore, 1991).

Flow rates were measured by an electromagnetic current meter located on the recirculation pipe and by the v-shaped weir connecting the downstream tanks in the tail-box. Flow depths and pressures were acquired by a series of piezometers located along the flume and a manual point gauge. Each of the flume cross-sections, spaced 30 cm apart, was monitored at 11 grid-points spaced 10 cm apart. The achievement of equilibrium conditions along a given stream reach was determined by verifying that the reach-scale bed trend would coincide with the reach-scale free surface trend. It was also double-checked by verifying that the reach-averaged unbalanced transport rates had disappeared (i.e., by verifying that input bed–load and output bed–load were equal and constant). The effect of the presence of the confining sidewalls, which was investigated by evaluating the mean cross-sectional shear stresses based on the sidewall correction proposed by Cheng and Chua (2005), proved to be always negligible.

Fig. 1. Picture of the experimental device.

5. Results and discussion

Figs. 2–6 show the equilibrium longitudinal variation of M (computed from Eq. (22) and the locally observed U and u_{max}) along with the equilibrium longitudinal variation of $|H_u|$ (computed from Eq. (25)). In each of the runs we analysed, the equilibrium reaches, characterized by fully emerged gravel bars, exhibited the higher (positive) values of the entropic parameter. Except for R1, where a relative maximum of $M\left(x, t_{eq}\right)$ appeared almost at flume outlet and outside the fully braided reach, all the pre-equilibrium M-values were negative. Furthermore, even the positive values were considerably smaller than those indicated in the literature as typical of regular and compact river sections.

Cross-sectional velocity entropy exhibited the lower and the higher values along the flume axis in correspondence of the equilibrium braided and unbraided reaches, respectively. Overall, based on the outcome of our laboratory experiments, it would seem that in gravel-bed braided rivers longitudinal equilibrium is mapped by a periodic-like spatial variation of normalized velocity entropy.

Fig. 7 shows the space/time dependent ratio of section-average to section-maximum velocity for the sample run R4, which considerably oscillated along the flume axis and was characterized by a well-defined peak at the equilibrium braided cross-sections (from 300 to 400 cm). This peak was already very evident at $t = 166$ h $= 0.64\, t_{eq}$. The maximum of function U/u_{max} was associated with the higher value of unit-width dimensionless bed–load rate (not shown), which practically was a Bernoulli (equilibrium/non-equilibrium) distribution (De Vincenzo et al., 2016). This result may be explained in terms of cause–effect relationship between relative increase in mean cross-sectional velocity and enhanced longitudinal sediment transport capacity along the equilibrium-braided reach. Indeed, by definition, river dynamical equilibrium is characterized by the perfect balance between locally available flow energy and flow energy required to convey the input sediment load. Conversely,

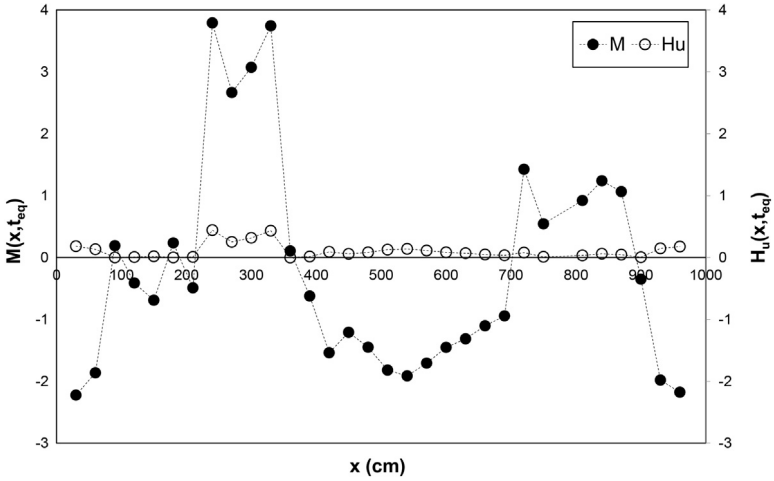

Fig. 2. Longitudinal variation of entropy and entropic parameter in run R1 at equilibrium.

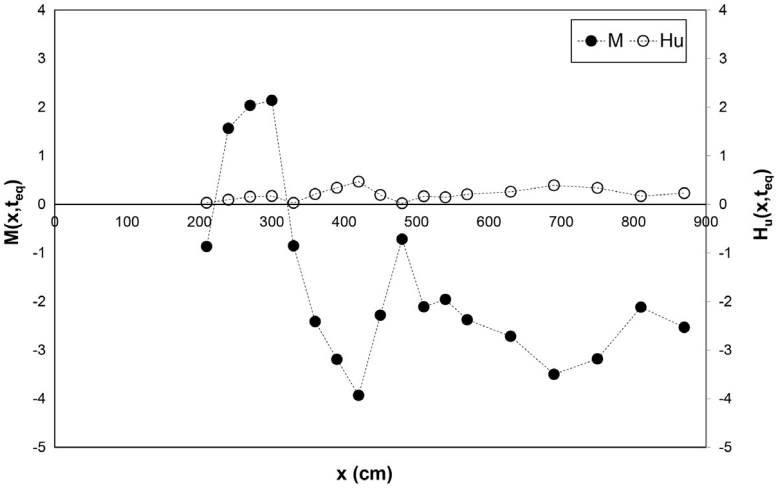

Fig. 3. Longitudinal variation of entropy and entropic parameter in run R2 at equilibrium.

along the non-equilibrium reaches, the unbalanced flow energy is employed for sediment erosion–deposition and residual bed modelling.

Fig. 8 shows along a 11.4 m reach in R4 the equilibrium normalized variance of velocity based on Eq. (26), the normalized variance of wetted bed elevation function based on Eq. (28), and a map of the difference between free surface and bed quotes. In the map, the white areas indicate the peaks of the emerged bed while the black areas indicate the deepest points of the submerged bed. As one can see, both the space-dependent normalized variances were characterized by a pseudo-periodical trend, which approximately followed bed profile undulations. Thus, both cross-sectional velocity and bed elevation, represented by space-dependent means and coefficients of variation, could be classified as non-stationary stochastic processes.

For a more complete statistical characterization of the de-trended elevation function $\widetilde{\delta}$ refer to Fig. 9, which shows at equilibrium in R4 the 3-D representation of the corresponding (experimentally

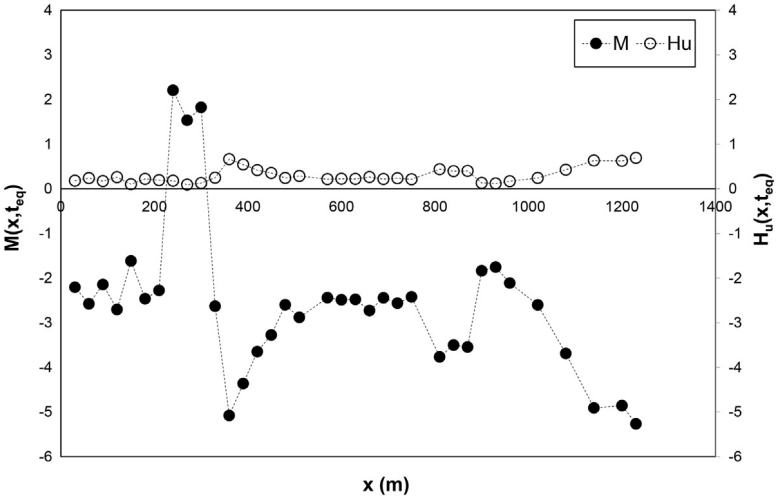

Fig. 4. Longitudinal variation of entropy and entropic parameter in run R3 at equilibrium.

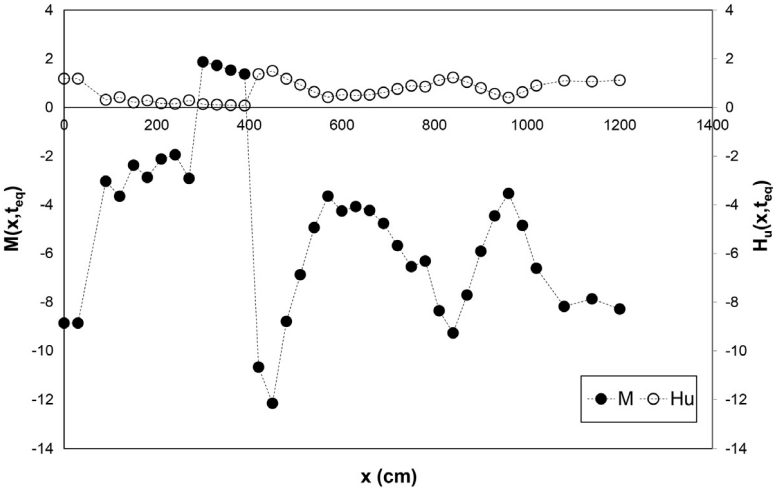

Fig. 5. Longitudinal variation of entropy and entropic parameter in run R4 at equilibrium.

reconstructed) spatial semi-variogram matrix:

$$\varepsilon_{\delta ij} = \varepsilon_{\delta}\left(x_i, x_j, t_{eq}\right) = \frac{1}{2B}\int_0^B \left[\widetilde{\delta}\left(x_i, y, t_{eq}\right) - \widetilde{\delta}\left(x_j, y, t_{eq}\right)\right]^2 dy. \tag{29}$$

As one can see, besides the pseudo-periodical oscillations, the matrix does not present constant values along the diagonals parallel to the principal diagonal ($\varepsilon_{\delta}(x_i, x_i, t_{eq}) = 0$), meaning that the variance of the increments depends on both sampling points' distance and absolute position.

Interesting enough, the maxima of velocity normalized variance corresponded to the minima of normalized bed elevation variance and vice versa, both in the equilibrium and in the pre-equilibrium reaches. Therefore, whereas mild transverse bed undulations that do not partialize the flow area and are associated with relatively reduced topographical variance determine a more heterogeneous

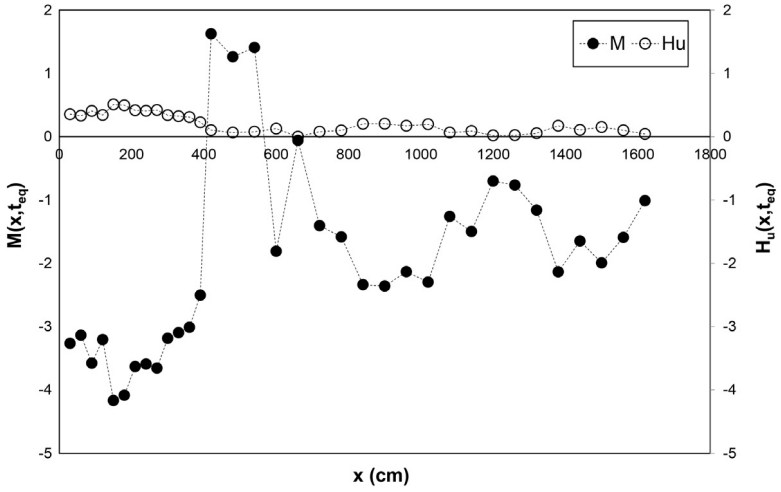

Fig. 6. Longitudinal variation of entropy and entropic parameter in run R9 at equilibrium.

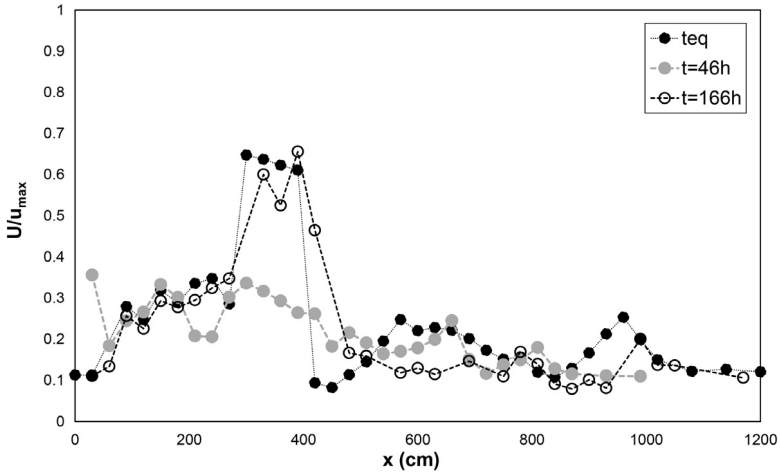

Fig. 7. Longitudinal variation of mean cross-sectional to section-maximum velocity ratio in run R4.

velocity distribution, the drastic reduction of flow area in correspondence of emerged bars causes the alignment of stream-lines, the attenuation of secondary currents and, hence, the homogenization of the velocity distribution. Indeed, the normalized velocity entropy as defined by Eq. (25), where $\ln[u_{\max}(x,t)]$ represents $H(u)$ in case of uniform probability density $f(u) = 1/u_{\max}$, can be interpreted as a measure of the deviation of the actual distribution from the uniform case. Since H_u is always negative, it means that the minima of $|H_u|$ in correspondence of the emerged bars, in phase with the minima of the normalized velocity variance, are associated with the minimum deviation from the uniform cross-sectional velocity distribution, for which $U/u_{max} = 0.5$.

These results are fully consistent with the physics of the phenomenon. As stated among the others by Grant (1997), "braided, gravel-bed rivers with slopes in excess of 0.01 tend to maintain critical flow in each of their braids over a range of discharges (Fahnestock, 1963; Schumm and Khan, 1972; Boothroyd and Ashley, 1975; Ergenzinger, 1987)". As shown in Table 1, except for a single run where

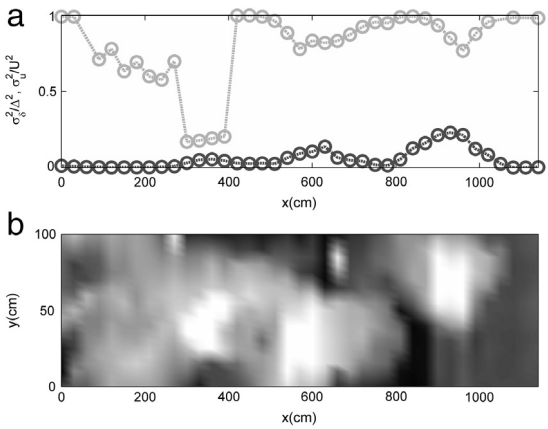

Fig. 8. (a) R4 Wetted bed elevation normalized variance (black circles) and velocity normalized variance (grey circles) at equilibrium; (b) R4 map of bed elevation minus free surface elevation at equilibrium.

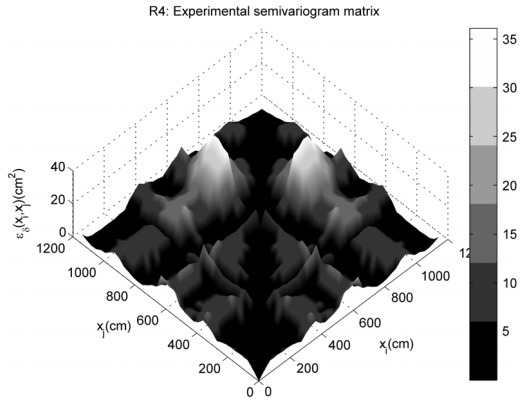

Fig. 9. Experimental semi-variogram matrix for the de-trended bed elevation function at equilibrium in R4.

$S_{eq} = 0.007$ (which is not far from 0.01), all our equilibrium slopes reach or exceed that value. A braided system can be interpreted as a sequence of macroscopic flow-section constrictions (De Vincenzo et al., 2016). As known from basic Hydraulics, in the presence of macroscopic flow-section narrowing the unit flow rate $q(x) = Q/b(x) = U(x)\,\overline{h}_b(x)$, where $b(x)$ indicates the varying cross-section free width and $\overline{h}_b(x) = A(x)/b(x)$, is close or exceeds its maximum possible value. For this reason, water flows across the free braids in critical conditions after upstream deepening, with the maximum allowable unit-width flow rate and the minimum relative energy sufficient to by-pass the bed constriction. At a given time, flow relative energy is given by

$$E(x) = \overline{h}_b(x) + \alpha(x)\frac{U^2(x)}{2g} = \overline{h}_b(x) + \alpha(x)\frac{q^2(x)}{2g\overline{h}_b^2(x)} \tag{30}$$

where g is the acceleration due to gravity and the scaling coefficient α, which accounts for the cross-sectional velocity heterogeneity, is given by (see also Chiu, 1991)

$$\alpha(x) = \frac{1}{U^3(x)} \int_0^{u_{\max}(x)} u^3 f(u|x)\, du = \\ = \frac{\{\exp[M(x)] - 1\}^2 \left\{\exp[M(x)]\left[M^3(x) - 3M^2(x) + 6M(x) - 6\right] + 6\right\}}{\{\exp[M(x)][M(x) - 1] + 1\}^3}. \tag{31}$$

In case of mildly heterogeneous cross-sectional distributions and small deviations about the mean cross-sectional velocity (formally, for $(u - U)/U \ll 1$), we obtain

$$\alpha(x) \cong 1 + 3\frac{\sigma_u^2(x)}{U^2(x)}. \tag{32}$$

Additionally, in terms of energy spatial derivative:

$$\frac{dE}{dx} = \frac{d\bar{h}_b}{dx} + \alpha(x)\frac{q(x)}{g\bar{h}_b^2(x)}\frac{dq}{dx} + \frac{d\alpha}{dx}\frac{q^2(x)}{2g\bar{h}_b^2(x)} - \alpha(x)\frac{q^2(x)}{g\bar{h}_b^3(x)}\frac{d\bar{h}_b}{dx} \\ = \left[1 - \alpha(x)\frac{q^2(x)}{g\bar{h}_b^3(x)}\right]\frac{d\bar{h}_b}{dx} + \alpha(x)\frac{q(x)}{g\bar{h}_b^2(x)}\frac{dq}{dx} + \frac{d\alpha}{dx}\frac{q^2(x)}{2g\bar{h}_b^2(x)}. \tag{33}$$

In critical conditions at the braided sections, one has $q = q_{max}$, $dq/dx = 0$ and $dE/d\bar{h}_b = 0$. Thus,

$$\bar{h}_{bc} = \sqrt[3]{\frac{\alpha q_{\max}^2}{g}} \tag{34}$$

and

$$\left.\frac{dE}{dx}\right|_{\bar{h}_{bc}} = \left.\frac{d\alpha}{dx}\right|_{\bar{h}_{bc}} \frac{q_{\max}^2}{2g\bar{h}_{bc}^2}. \tag{35}$$

Before and after the braided sections, relative energy is lower than in the braids, leading to $dE/dx|_{\bar{h}_{bc}} = 0$. Therefore, according to the experimental observations, critical flow in the braids implies spatially minimum velocity normalized variance ($d\alpha/dx \cong 3d\left(\sigma_u^2(x)/U^2(x)\right)/dx = 0$).

Note that the incipient emersion of bars in the pre-equilibrium reach (see the two higher downstream peaks of normalized bed elevation variance in Fig. 8) was accompanied by two minima of the normalized velocity variance that are markedly less pronounced than the minimum in the equilibrium reach, where the bar was already fully emerged. A physical explanation for that behaviour may reside in the occurrence of a hydro-dynamical discontinuity represented by the emersion of bars.

Finally, as an example of entropy spatio-temporal evolution toward morphological equilibrium, Fig. 10 displays the absolute value of function $H_u(x, t)$ at $t = 46$ h, $t = 166$ h and $t = t_{eq} = 261$ h in run R4. As one can see, in the future equilibrium reach (300 cm $\leq x \leq$ 1000 cm) bed evolution occurred by both entropy minima/maxima appearance and growth (which was the prevailing morphological process in non-equilibrium conditions — from 46 to 166 h) and entropy minima/maxima upstream migration (which was the prevailing process in near-equilibrium conditions — from 166 to 261 h).

6. Conclusions

Braided-bed rivers typically modify their plan-form in response to changes in flow velocity distribution that make their morphology extremely complex. In the present study, an experimental investigation was conducted for the statistical characterization of bank-full flow spatial structure in braided gravel beds evolving toward dynamical equilibrium. Based on the conditional cross-sectional maximization of the velocity information entropy according to a generalization of Chiu's approach (1991), the longitudinally varying cross-sectional entropy and the corresponding variance were computed as a function of a single representative parameter. The results of the analysis indicate the following. Unlike the case of regular cross-sections and near-uniform flow conditions, already extensively treated in the literature, the presence of intertwined braids was associated with a pseudo-periodical variation of both normalized velocity entropy and variance. Bed evolution toward equilibrium occurred by both entropy minima/maxima appearance and growth and entropy minima/maxima

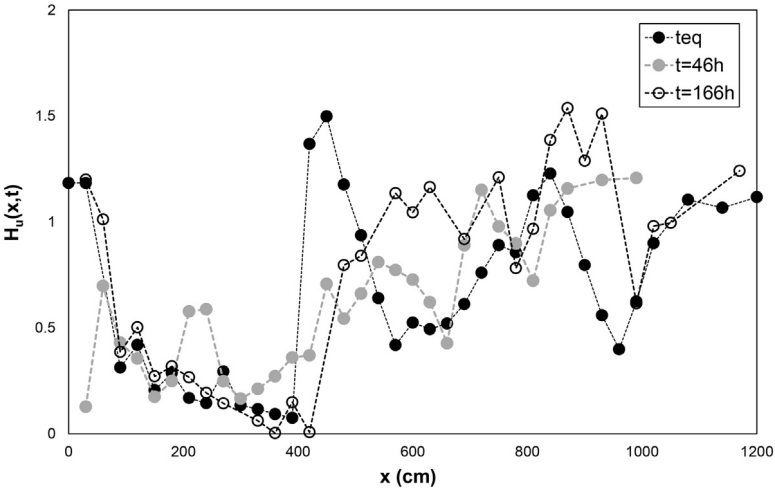

Fig. 10. Velocity entropy spatio-temporal evolution in R4.

upstream migration. The first morphological process prevailed in the pre-equilibrium stages; the second prevailed in near-equilibrium conditions.

Additionally, the range of the ratio of velocity cross-sectional average to velocity cross-sectional maximum was rather wide and characterized by values that are generally smaller than those belonging to compact channel sections. The larger values were concentrated in the equilibrium reaches, characterized by the complete emersion of bars. Velocity normalized variance exhibited local minima in correspondence of incipient bar emersion and markedly more pronounced minima in correspondence of fully emerged bars and flow bifurcation, likely highlighting the occurrence of a hydrodynamical discontinuity at braided equilibrium. The longitudinal pseudo-periodicity exhibited by the normalized velocity variance presented a phase shift with respect to the bed elevation normalized variance. Therefore, whereas mild transverse bed undulations that do not partialize the flow area and are characterized by relatively reduced topographical variance determine a more heterogeneous velocity distribution, the drastic reduction of flow area in correspondence of emerged bars causes the alignment of stream-lines, the attenuation of secondary currents and, hence, the homogenization of velocity cross-sectional distribution.

The proposed approach allows estimating all velocity central moments m_n ($n \geq 2$) by Eqs. (19), (22) and (27) and simple flow-depth measurements. Specifically, the equation of continuity yields the mean cross-sectional velocity for the given flow rate:

$$U(x,t) = \frac{Q}{A(x,t)} = \frac{Q}{B\overline{h}(x,t)}. \tag{36}$$

Prandtl–von Kàrmàn's logarithmic law (19) gives the maximum of the distribution:

$$\frac{u_{\max}(x,t)}{u_*(x,t)} = \frac{1}{\kappa}\ln\left[\frac{h_{\max}(x,t)}{2D_{50}}\right] + 8.5. \tag{37}$$

Eq. (22) provides the space–time varying entropic parameter $M(x,t)$. Finally, from the probability density function in Eq. (27), one can compute the required cross-sectional velocity statistics:

$$m_n(x,t) = \int_0^{u_{\max}(x,t)} [u(x,y,z,t) - U(x,t)]^n f(u|x,t)\,du. \tag{38}$$

Once the velocity field is completely characterized, one might use the results to predict or monitor transport of sediment (bed and suspended load), chemical contaminants and even floating logs in bank-full flow conditions by Eulerian or Lagrangian stochastic numerical simulations.

References

Ashmore, P.E., 1991. How do gravel-bed rivers braid? Can. J. Earth Sci. 28, 326–341.

Bertoldi, W., Ashmore, P., Tubino, M., 2009. A method for estimating the mean bed load flux in braided rivers. Geomorphology 103, 330–340. http://dx.doi.org/10.1016/j.geomorph.2008.06.014.

Boothroyd, J.C., Ashley, G.M., 1975. Processes, bar morphology, and sedimentary structures on braided outwash fans, northeastern Gulf of Alaska. In: Jopling, A.V., McDonald, .C. (Eds.), Glaciofluvial and Glaciolacustrine Sedimentation. SEPM Spec. Publ. 23, Soc. of Econ. Paleontol. and Miner., Tulsa, Okla, pp. 193–222.

Cheng, N.-S., Chua, L.H.C., 2005. Comparison of sidewall correction of bed shear stress in open channel flows. J. Hydraul. Eng. 131 (7), 605–609. http://dx.doi.org/10.1061/(ASCE)0733-9429(2005)131:7(605).

Chiu, C.L., 1991. Application of entropy concept in open-channel flow study. J. Hydraul. Eng. 117 (5), 615–628.

Chiu, C.L., Chiou, J.D, ., 1986. Structure of 3-D flow in rectangular open channels. J. Hydraul. Eng. 112, 1050–1068.

Chiu, C.L., Said, C.A.A., 1995. Maximum and mean velocities and entropy in open-channel flow. J. Hydraul. Eng. 121 (1), 26–35.

De Vincenzo, A., Brancati, F., Pannone, M., 2016. An experimental analysis of bed load transport in gravel-bed braided rivers with high grain Reynolds numbers. Adv. Water Resour. 94, 160–173. http://dx.doi.org/10.1016/j.advwatres.2016.05.007.

Ergenzinger, P., 1987. Chaos and order: The channel geometry of gravel bed braided rivers. In: Ahnert, F. (Ed.), Geomorphological Models. In: Catena Suppl., vol. 10, Catena Verlag, Cremlingen-Destedt, Germany, pp. 85–98.

Fahnestock, R.K., 1963. Morphology and hydrology of a glacial stream - White River, Mount Rainier, Washington. U.S. Geol. Surv. Prof. Pap. 422-A, 70 pp.

Gelfand, I.M., Fomin, S.V., 2000. Calculus of Variations. Dover, U.S.A., p. 232. Translated and Edited By R.A. Silverman.

Grant, G.E., 1997. Critical flow constrains flow hydraulics in mobile-bed streams: A new hypothesis. Water Resour. Res. 33, 349–358.

Gray, R., 2013. Entropy and Information Theory. Springer New York, ISBN: 1475739834, p. 332. http://dx.doi.org/10.1007/978-1-4757-3982-4.

Greco, M., Mirauda, D., 2015a. An entropy based velocity profile for steady flows with large-scale roughness. In: Lollino, G., Arattano, M., Rinaldi, M., Giustolisi, O., Marechal, J.-C., Grant, G.E. (Eds.), Engineering Geology for Society and Territory, River Basins, Reservoir Sedimentation and Water Resources, vol. 3. Springer International Publishing, Switzerland. http://dx.doi.org/10.1007/978-3-319-09054-2_128.

Greco, M., Mirauda, D., 2015b. Entropy parameter estimation in large-scale roughness open channel. J. Hydrol. Eng. 20 (2), 04014047-1–04014047-6. http://dx.doi.org/10.1061/(ASCE)HE.1943-5584.0001009.

Greco, M., Mirauda, D., Plantamura Volpe, A., 2014. Manning's roughness through the entropy parameter for steady open channel flows in low submergence. Procedia Eng. 70, 773–780. http://dx.doi.org/10.1016/j.proeng.2014.02.084.

Jaynes, E.T., 1957. Information theory and statistical mechanics. Phys. Rev. 106, 620–630.

Jaynes, E.T., 1983. Bayesian spectrum and chirp analysis. In: Smith, C.R., Erickson, G.J. (Eds.), Third Workshop on Maximum-Entropy and Bayesian Methods. D. Reidel, Norwell, Mass, pp. 1–55.

Jaynes, E.T., 1984. Prior information and ambiguity in inverse problems. SIAM AMS Proc. 14, 151–166.

Kitanidis, P.K., 1994. The concept of the dilution index. Water Resour. Res. 30, 2011–2026.

Kittel, C., Kroemer, H., 1980. Thermal Physics. W.E. Freeman, New York, p. 473.

Kreibich, H., Piroth, K., Seifert, I., Maiwald, H., Kunert, U., Schwarz, J., Merz, B., Thieken, A.H., 2009. Is flow velocity a significant parameter in flood damage modelling? Nat. Hazards Earth Syst. Sci. 9, 1679–1692. www.nat-hazards-earth-syst-sci.net/9/1679/2009/.

Leopold, L.B., Langbein, W.B., 1962. The concept of entropy in landscape evolution, Theoretical papers in the hydrologic and geomorphic sciences, Geological Survey Professional Paper 500-A, U.S. Government Printing Office, Washington, A1-A20.

Luo, H., Singh, V.P., 2011. Entropy theory for two-dimensional velocity distribution. J. Hydraul. Eng. 16, 303–315. http://dx.doi.org/10.1061/(ASCE)HE.1943-5584.0000319. ASCE.

Mirauda, D., Greco, M., Moscarelli, P., 2011. Practical method for flow velocity measurements in fluvial sections. In: Brebbia, C.A. (Ed.), River Basin Management VI. In: WIT Transactions on Ecology and the Environment, vol. 146, Wessex Institute of Technology, England, pp. 355–367. http://dx.doi.org/10.2495/RM110301.

Moramarco, T., Ammari, A., Burnelli, A., Mirauda, D., Pascale, V., 2008. Entropy theory application for flow monitoring in natural channels. In: Sanchez-Marrè, M., Béjar, J., Comas, J., Rizzoli, A.E., Guariso, G. (Eds.), Proc. IEMSs 4th Biennial Meeting International Congress on Environmental Modelling and Software. (IEMSs 2008), Int. Environmental Modelling and Software Society, Barcelona, Catalonia, Spain, pp. 430–437.

Nezu, I., Tominaga, A., Nakagawa, H., 1993. Field measurements of secondary currents in straight rivers. J. Hydraul. Eng. 119, 598–614. http://dx.doi.org/10.1061/(ASCE)0733-9429(1993)119:5(598).

Pannone, M., 2010a. Transient hydrodynamic dispersion in rough open channels: theoretical analysis of Bed-Form effects. J. Hydraul. Eng. 136, 155–164. http://dx.doi.org/10.1061/_ASCE_HY.1943-7900.0000161. ASCE.

Pannone, M., 2010b. Effect of nonlocal transverse mixing on river flows dispersion: A numerical study. Water Resour. Res. 46, W08534. http://dx.doi.org/10.1029/2009WR008100.

Pannone, M., 2012a. Longitudinal Dispersion in River Flows Characterized by Random Large-Scale Bed Irregularities: First-Order Analytical Solution. J. Hydraul. Eng. 138, 400–411. http://dx.doi.org/10.1061/(ASCE)HY.1943-7900.0000537. ASCE.

Pannone, M., 2012b. On the exact analytical solution for the spatial moments of the cross-sectional average concentration in open channel flows. Water Resour. Res. 48, W08511. http://dx.doi.org/10.1029/2011WR011665.

Pannone, M., 2014. Predictability of tracer dilution in large open channel flows: Analytical solution for the coefficient of variation of the depth-averaged concentration. Water Resour. Res. 50, 2617–2635. http://dx.doi.org/10.1002/2013WR013986.

Pannone, M., De Vincenzo, A., 2015. Stochastic numerical analysis of anomalous longitudinal dispersion and dilution in shallow decelerating stream flows. Stoch. Environ. Res. Risk. Assess. 29, 2087–2100. http://dx.doi.org/10.1007/s00477-014-1006-0.

Pannone, M., Kitanidis, P.K., 1999. Large-time behavior of concentration variance and dilution in heterogeneous formations. Water Resour. Res. 35, 623–634.

Parker, G., 2003. Persistence of sediment lumps in approach to equilibrium in sediment-recirculating flumes. In: Proceedings XXX International Association of Hydraulic Research Congress, Thessaloniki, Greece, Agust 24-29, p. 8.

Peakall, J., Ashworth, P., Best, J.L., 1996. Physical modelling in fluvial geomorphology: principles, applications and unresolved issues. In: Rhoads, L.B, Thorn, E.C. (Eds.), The Scientific Nature of Geomorphology. Wiley & Sons, Chichester, pp. 221–253.

Schumm, S.A., Khan, H.R., 1972. Experimental study of channel patterns. Geol. Soc. Am. Bull. 83, 1755–1770.

Shannon, C.E., 1948. A mathematical Theory of Communication. Bell Syst. Tech. J. 27, 623–656.

Viparelli, M., Pica, M., 1967. Streams in Large Alluvial Beds of High Slope. XII I.A.H.R. In: International Congress, Fort Collins (downloadable at http://www.diia.unina.it/collana02.html).

Woodbury, A.D., Ulrich, T.J., 1993. Minimum relative entropy: Forward probabilistic modelling. Water Resour. Res. 29, 2847–2860.

Yalin, M.S., 1971. Theory of Hydraulic Models. Macmillan, New York, p. 266.

Yalin, M.S., 1992. River Mechanics. Pergamon Press, Oxford UK.

Young, W., Davies, T., 1991. Bedload transport in braided gravel-bed river model. Earth Surf. Process. Landf. 16, 499–511. http://dx.doi.org/10.1002/esp.3290160603.

Young, W.J., Warburton, J., 1996. Principles and practice of hydraulic modelling of braided gravel-bed rivers. J. Hydrol. 35 (2), 175–198.

Zarn, B., 1997. Einfluss der flussbettbreite auf die wechselwirkung zwischen abfluss, morphologie und geschiebetransportkapazität. In: Vischer, D. (Ed.), VAW Mitteilung 154, Laboratory of Hydraulics, Hydrology and Glaciology. (VAW), ETH Zurich, Switzerland, (in german).